Feasibility of head-tilted brain scan to reduce susceptibility-induced signal loss in the prefrontal cortex in gradient echo-based imaging

Seulki Yoo [a,b,1], Hayoung Song [a,b,c,1], Seong-Gi Kim [a,b], Won Mok Shim [a,b,*], Seung-Kyun Lee [a,b,d,*]

[a] Center for Neuroscience Imaging Research, Institute for Basic Science (IBS), Suwon 16419, South Korea
[b] Department of Biomedical Engineering, Sungkyunkwan University, Suwon 16419, South Korea
[c] Department of Psychology, University of Chicago, Chicago, IL, USA
[d] Department of Physics, Sungkyunkwan University, Suwon 16419, South Korea

ARTICLE INFO

ABSTRACT

Susceptibility-induced static field (B_0) inhomogeneity near the nasal cavity degrades high-field MRI image quality. Many studies have addressed this problem by hardware- or sequence-based methods to improve local B_0 shimming or minimize the impact of inhomogeneity. Here, we investigate the feasibility of the head-tilted brain scan as an easily accessible way to reduce B_0 inhomogeneity and associated gradient echo signal loss in the prefrontal cortex (PFC). We exploit the fact that the region of intense local B_0 gradient can be steered away from the PFC by head reorientation with respect to the main magnetic field. We found that the required chin-up head tilting by a substantial angle (> 30°) can be readily achieved for a group of healthy subjects when their back was raised by about 10 cm. Eleven subjects were scanned at 3T, using a standard 20 channel head-neck coil, for whole-head B_0 mapping and gradient-echo EPI-based functional MRI (fMRI) performing a reward-punishment task in normal and tilted head orientations. Additionally, multi-echo gradient echo and resting-state fMRI scans were performed on six subjects in both orientations. Head-tilted sessions, which lasted for at least 20 min, were well-tolerated by all subjects and demonstrated a marked reduction of localized signal loss in the gradient echo-based images and EPI images in the PFC compared to normal orientation scans. Imaging in tilted orientation reduced the group-averaged B_0 standard deviation and peak B_0 gradient in the orbital gyrus beyond what was possible with simulated 3rd order shimming. The behavioral performance in the head-tilted fMRI scans indicated that the subjects were able to perform a cognitive task with little difficulty, and the tilted fMRI scans successfully produced a robust whole-brain functional activation map consistent with the literature. Our study proposes that the back-raised, head-tilted imaging can benefit the shimming of the prefrontal brain regions while being compatible with moderate-length neuroimaging scans on healthy, cooperating subjects.

1. Introduction

In high-field MRI, tissue-air susceptibility difference at the boundaries of the sinus and nasal cavities creates static-field (B_0) inhomogeneity that degrades the image quality in the nearby brain regions. Measurements (Cusack et al., 2005) indicate that the susceptibility-induced B_0 gradient in the prefrontal cortex (PFC) directly above the nasal cavity is on the order of 5 G/m ≈ 21 Hz/mm at 3T. With such a gradient, a voxel of size 2 mm will completely dephase at an echo time (TE) of 24 ms in gradient-echo based imaging. While a short TE will mitigate this, relatively long echo times are needed in, for example, T_2^* contrast imaging, R_2^* mapping, and phase-based local frequency shift measure-

ments as in quantitative susceptibility mapping (QSM) (Schweser et al., 2011; Yang et al., 2018).

Gradient-echo signal loss due to intra-voxel dephasing in the local B_0 gradient cannot be recovered by post-processing alone. Several methods have been proposed to address the source of the loss, namely to improve local B_0 shimming, through (i) higher-order harmonic shims (Clare et al., 2006; Kim et al., 2007), (ii) local shim coils (Hsu and Glover, 2005; Juchem et al., 2010), and (iii) local passive shimming (Cusack et al., 2005; Yang et al., 2011). While helpful, these shim approaches often require additional hardware that is not routinely available. Dynamic slice-by-slice shim (Sengupta et al., 2011) allows low-order shim coils to effectively shim higher-order fields one slice at a time, but such a scheme is limited to two-dimensional scan sequences.


In fMRI, the signal in the orbitofrontal region is sometimes recovered by a 'z-shim' technique (Constable, 1995) that specifically targets B_0 gradient in the slice direction. However, such a technique increases the scan time depending on the number of compensated slices (Du et al., 2007).

It has been noted early on that B_0 inhomogeneity due to the nasal cavity has significant head orientation dependence with respect to the main field, and chin-up head tilting improves B_0 homogeneity in the PFC (Heberlein and Hu, 2001). Tyszka and Mamelak (2002) experimentally measured regional and whole-brain B_0 standard deviations at head pitch angles in the range of ±30°, to find significant decrease of B_0 variation (linewidth) in the PFC as the angle increased. In non-human primate imaging, scans in a 'sphinx' position was recommended based on favorable B_0 profiles in the head (Valette et al., 2006). To our knowledge, there are few reports on translating B_0 homogeneity improvement by head reorientation to standard human neuroimaging scans. This contrasts with the extensive literature on applications of sequence- and hardware- based shimming strategies to human fMRI in the orbitofrontal cortex (Constable and Spencer, 1999; Deichmann et al., 2003; Du et al., 2007; Glover, 1999). One reason for this, presumably, is the perceived difficulty of maintaining an unconventional head orientation inside a conventional, cylindrical-bore scanner. Any benefit of increased B_0 homogeneity has to be balanced against the potential complexity in subject handling. On the other hand, if an acceptable subject handling workflow can be devised to facilitate head-tilted imaging, and if such imaging offers clear improvements in B_0 homogeneity and image quality, the advantage of being able to recover signal in the prefrontal cortex without using special hardware, modified sequences, or additional scan time, would be appealing.

The purpose of this study is twofold. First, we report that by elevating the subject's torso and letting the head drop into a standard clamshell type array coil, an anterior-posterior head-tilt angle up to and in excess of 45° is readily achievable and can be maintained for a meaningful (20 min or more) neuroimaging scan session. This was the case for a group of seventeen healthy subjects recruited in our study. In particular, eleven subjects participated in and completed task-based fMRI scans without being severely distracted by the new position. Second, we report that the previously published (Tyszka and Mamelak, 2002) B_0 homogeneity improvement with increased head pitch angle continued well past 30° to greatly reduce intravoxel dephasing near the nasal cavity at an angle as large as >50°. The B_0 improvement made a direct impact on signal recovery in EPI and multi-echo gradient echo scans. Overall, we found that for the subject group and scanner environment used, head-tilted brain imaging was practical and beneficial for the tested neuroimaging scans.

2. Theory

Inside an MRI magnet, the tissue-air boundary of the nasal cavity becomes a surface of discontinuity in magnetization whose direction is set by the applied magnetic field (B_{app}). The secondary magnetic field caused by such magnetization, therefore, depends on the orientation of B_{app} with respect to the cavity. This can be illustrated by a simple geometrical model (Fig. 1A). Here, a sphere with a positive relative susceptibility (+9 ppm) models an air cavity inside a uniform diamagnetic material crudely representing the tissue in the head. The magnetic field vector induced by the sphere and its projection along B_{app} (which is what matters in MRI) rotates with B_{app}, parameterized by an angle θ. In Fig. 1A, this means that a region of interest (ROI) fixed in the subject's frame of reference (black dotted rectangle) will see strongly θ-dependent B_0 patterns. For example, the sphere-induced field along the B_{app} direction is zero on a cone that makes 54.74° (magic angle) with B_{app}. This observation suggests that change of relative orientation between the nasal cavity and the main magnetic field can significantly alter the B_0 distribution in the prefrontal cortex (Heberlein and Hu, 2001). In particular, head tilting close to the magic angle may greatly reduce the B_0 gradient in the region (black dashed and red lines in Fig. 1C).
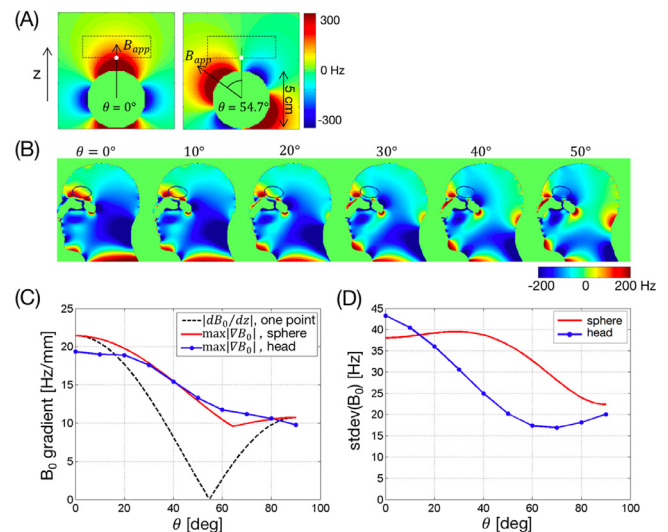
Fig. 1. Simulated B_0 maps around a sphere (A) and in a human head model (B), for different orientations of the main magnetic field (B_{app} = 3T). (C) Dependence of the B_0 gradient on the main-field orientation. Dashed black line indicates the z-directional (defined in the subject's coordinate system) gradient at the location of the white dot in (A). Red and blue traces indicate the maximum gradient magnitudes in the rectangular region of interest marked by black dotted lines in (A), and an ellipse in (B). (D) Standard deviation of B_0 in the same regions of interest.

3. Materials and methods

3.1. Simulation

A voxelated human head-and-neck phantom was extracted from the extended cardiac-torso (XCAT) model (https://olv.duke.edu/industry-investors/available-technologies/xcat/) (Segars et al., 2010) at 1 mm isotropic resolution. The model was simplified to a binary susceptibility mask, with all the tissue types given a susceptibility of −9 ppm, while all the other voxels were set to 0 ppm. While simplified, this model captures the main aspect of B_0 disturbance caused by the tissue-air interface. The susceptibility-induced B_0 maps for different applied field directions were calculated with an in-house developed code based on susceptibility voxel convolution (Jenkinson et al., 2004; Yoder et al., 2004; Lee et al., 2018). The method computes B_0 from circular convolution between the susceptibility map and a voxel-integrated dipolar field kernel. This method is known to avoid Gibbs ringing (Cheng et al., 2009; Lee et al., 2018), which is important for B_0 gradient calculation as is done in this work. In the model calculation, the applied field direction was changed by rotating it anteriorly in the sagittal plane by a positive angle θ. The relative orientation change between B_{app} and the head corresponds to chin-up head tilting in an MRI scan. All numerical calculations were performed in Matlab (MathWorks, Natick, MA, USA).

3.2. Scan

All scans followed a human study protocol approved by the Institutional Review Board (IRB) of Sungkyunkwan University. The healthy subjects were recruited and scanned in a 3T scanner (Magnetom Prisma, Siemens Healthineers, Erlangen, Germany). The scanner was equipped with full 2nd order shim coils which were utilized to shim B_0 in the head at the start of each scan session. Eleven subjects (5 males, 6 females, age range = 19–28) participated in B_0 mapping and task-based fMRI scans (Experiment 1). In addition, six subjects (3 males, 3 females, age range = 21–32) were scanned with multi-echo gradient echo and resting state fMRI sequences (Experiment 2). These subjects had a normal or corrected-to-normal vision and were monetarily compensated for
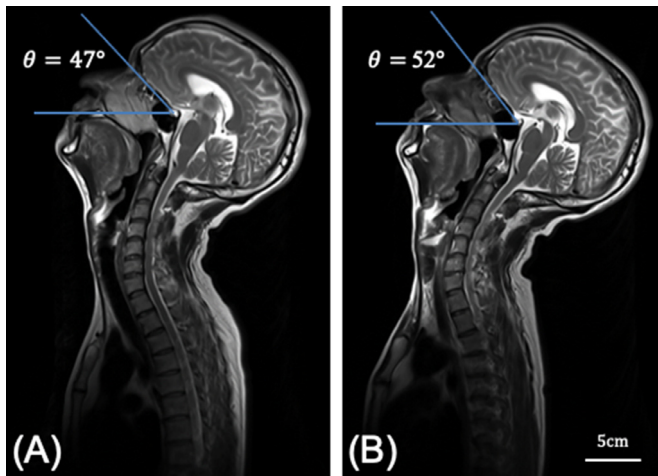
Fig. 2. Sagittal T_2-weighted images of a subject with low (A, 5 cm) and high (B, 12 cm) back support paddings. With higher padding, larger head tilt angles (52° vs. 47° in this example) could be obtained with less neck strain. These images were obtained with a 20 channel head-neck coil and a 24 channel spine coil.

their participation. The scan parameters for both experiments are listed in Table 1.

The imaging FOV was manually placed on a sagittal localizer image such that the base of the rectangular FOV was approximately parallel to the inferior boundary of the prefrontal cortex. For the head-tilted scans, when the FOV was prescribed more than 45° rotated from the default orientation, the nominal scan plane switched automatically from axial to coronal. This was not a problem as long as the phase encoding direction was kept consistent between the normal and head-tilted scans.

All scans used the standard, vendor-provided head-and-neck coil with 20 receiver channels. The coil had a clam-shell design with detachable posterior and anterior halves. The posterior half was firmly plugged into the patient table with no flexibility; all the head orientations reported here were within the confine of the fixed interior space of the coil housing. The inside dimensions of the coil where the head was placed were 23 and 25 cm in the left-right and anterior-posterior directions, respectively.

3.2.1. Subject handling

Each subject was scanned in two head orientations — normal and tilted — in separate sessions, with scan orders counter-balanced. In each session, the subject maintained the head orientation for at least 20 minutes. In a normal orientation scan, the subject kept a conventional, head-first supine position with a direct upward-gazing head posture, with a 2 cm thick foam pad placed under the back of the head. In a head-tilted scan, the subject's torso was elevated 10–12 cm using flat foam pads (Fig. 2). With the back on the padding, the subject dropped his/her head into the posterior half of the clam-shell coil, lightly touching the housing's bottom via a thin (5 mm) foam pad. This arrangement naturally induced a chin-up head posture where the subject's line of view was at about 45° from the vertical direction toward the back of the scanner. To prevent motion, paddings were applied liberally under the neck, on the cheeks, and between the forehead and the coil housing. The head-tilt angle was adjusted to allow the subject's elevated chin to stay clear from or gently touch the opening portion of the coil housing.

In our setup and experience, the chin-coil interference limited the maximum head-tilt angle. No attempt was made to impose a precise or predetermined tilt angle. Our procedure resulted in tilt angles in the range of 28° to 53° (mean 43.24°), relative to each subject's respective normal orientation. All subjects had a clear view to a screen at the end of the bore, via a mirror making an appropriate angle (45° and 20° for normal and head-tilted scans, respectively) with respect to the horizontal

Table 1
Scan parameters of the sequences used to compare normal and head-tilted imaging.

	Experiment 1			Experiment 2		
	B_0 map	EPI	MPRAGE	Multi-echo gradient echo	EPI	MPRAGE
acquisition type	2D axial	2D axial	3D axial	3D axial	2D axial	3D axial
TR (ms)	23	4000	2200	47	4000	2200
TE (ms)	2.9, 5.4	37	2.44	7 to 42 in 5 ms steps	37	2.43
flip angle (°)	15	90	8	20	90	8
bandwidth (Hz/px)	630	2120	250	240	2120	250
slice thickness (mm)	2.0	2.0	1.0	0.8	2.0	1.0
matrix size	64 × 54 × 50	118 × 104 × 60	256 × 256 × 256	512 × 352 × 52	118 × 104 × 60	190 × 224 × 192
field of view (mm³)	220 × 185 × 100	236 × 208 × 120	256 × 256 × 256	270 × 186 × 96	236 × 208 × 120	190 × 224 × 192
voxel size (mm³)	3.43 × 3.43 × 2.0	2.0 × 2.0 × 2.0	1.0 × 1.0 × 1.0	0.53 × 0.53 × 0.8	2.0 × 2.0 × 2.0	1.0 × 1.0 × 1.0
acceleration factor (phase direction)	2	2	2	2	2	2
acquisition time (min:sec)	0:26	5:24 (81 volumes, repeated twice)	5:36	8:47	13:40 (205 volumes)	4:16
others		echo spacing = 0.56 ms	TI = 925 ms		echo spacing = 0.56 ms	TI = 963 ms

Abbreviations. MPRAGE: magnetization-prepared rapid acquisition with gradient echo, TI: Inversion time, TR: repetition time, TE: echo time.

plane. The visual stimuli for fMRI scans were projected from the back of the scanner onto the screen, from a Propixx projector (VPixx Technologies, Saint-Bruno, Canada) (1920 × 1080 resolution, 1440 Hz). After the scan, all subjects were asked to rate their level of comfort during the two scan sessions on the scale of 1 (very uncomfortable) to 5 (very comfortable).

3.2.2. Experiment 1

Eleven subjects underwent a set of scans in each head orientation: B_0 mapping, T_1-weighted magnetization-prepared rapid gradient echo (MPRAGE), and 2D gradient echo EPI-based functional MRI scans with a probabilistic reversal learning task. The task, modified from O'Doherty et al. (2001), was implemented as the reward-punishment localizer task during fMRI scans. This paradigm was used because previous findings (O'Doherty et al., 2001) reported consistent activation within the ventro-medial prefrontal cortex (vmPFC), during the presentation of monetary rewards, compared to monetary loss. On each trial, two-colored fractal stimuli were presented side by side in the middle of the screen for 2 s and were followed by a 1 s period of the blank screen. The images were randomly assigned to be a correct or incorrect choice; making a correct choice elicited monetary reward 80% of trials and monetary punishment 20% of trials, and vice versa for an incorrect choice. Subjects were instructed to make a binary choice on the correct stimulus using a button press, during a 2 s period of stimuli presentation. When subjects made a correct choice, it was more likely to be followed by an image of 500 KRW appearing on the screen for 4 s ('reward' trials), and when subjects made an incorrect choice, it was more likely to be followed by an image of 500 KRW with a red X sign appearing on the screen for 4 s ('punishment' trials). There was 1 s intertrial interval. The contingency associated with the images was reversed when the subjects made correct choices for three consecutive trials. Subjects were unaware of the exact probabilities and rules of reversal but were instructed to adjust their strategy on a trial-by-trial basis. Each run consisted of 40 trials, lasting 5 min 24 s. Two runs were performed in each orientation session. Stimulus presentation and response recording were controlled with Matlab and Psychtoolbox (Brainard, 1997; Pelli, 1997).

3.2.3. Experiment 2

Six subjects underwent the following set of scans in each head orientation: multi-echo gradient echo, T_1-weighted MPRAGE, and a single run of 2D gradient-echo EPI-based resting-state fMRI. The fMRI scan lasted for 13 min 40 s. The subjects were instructed to keep their eyes open at all times and to fixate at the center of the screen.

3.3. Data analysis

Preprocessing, image registration and analysis were performed with FSL (Jenkinson et al., 2012), AFNI (Cox, 1996), and Matlab.

3.3.1. B_0 map data analysis

B_0 maps were obtained from the difference between the gradient-echo phase images at two echo times (TE = 2.9 ms and 5.4 ms). B_0 gradient amplitudes were calculated from the vector sum of the nearest neighbor differences in the three grid directions. To quantify the B_0 inhomogeneity in the PFC, an ROI mask corresponding to the orbital gyrus in the Brainnetome atlas (Fan et al., 2016) was registered to the B_0 maps of each subject in both orientations. The masks extracted from the normalized brain space were reverse-transformed to each subjects' native brain space. Additionally, the brain mask for the B_0 map was eroded by two pixels to avoid partial volume effect and unreliable phase values near the boundary. The standard deviation of B_0 and the peak B_0 gradient, defined as the average of the top 1% B_0 gradient values (consisting typically of 20 voxels) in the ROI, were extracted for comparison between normal and tilted orientation scans.

In order to investigate the extent to which the B_0 homogeneity is improved by high-order volumetric shimming, the B_0 maps in the normal

head orientation were fitted with spherical harmonic functions up to the 3rd order (total 16 functions). The gradient and the standard deviation of the residual (synthetically shimmed) B_0 maps were calculated within the orbital gyrus mask as described above.

3.3.2. fMRI data analysis

Both normal and tilted orientation EPIs were aligned to a normally-oriented T_1-weighted image. Motion correction was applied with 6 linear degrees of freedom (3 rotation and 3 translation parameters). None of the subjects showed severe head motion, thresholded at framewise displacement (FD) < 0.5 (Power et al., 2012, 2014).

The temporally-averaged signal intensity (mean signal) and across-time variance of the signal (temporal SD) were extracted from each voxel in multiple ROIs. The temporal signal-to-noise ratio (tSNR) was computed as the ratio of the mean signal to the temporal SD. The tSNR of each voxel was then averaged within the ROIs of the orbital gyrus, a 'V-shaped' PFC, and the whole brain. The 'V-shaped' PFC refers to a typical V-shaped hypointense region near the nasal cavity on the axial view of normal orientation EPIs; it was manually masked to an individual-specific ROI and was applied to the spatially aligned, tilted EPIs. The orbital gyrus mask was extracted from the Brainnetome atlas. Paired t-tests were performed for each ROI to compare the mean signal, temporal SD, and tSNR between the normal and tilted orientations, and the p-values were corrected for the number of ROIs (=3) using the false discovery rate (FDR).

To compare the task-based fMRI activation maps from the head-tilted scans with the normally positioned scans, we aligned the functional EPIs of all subjects in Experiment 1 to the MNI template brain. Spatial smoothing was applied using a Gaussian kernel with full-width at half-maximum of 4 mm. The blood oxygenation level-dependent (BOLD) signals were normalized to the mean image intensity and linearly de-trended. A generalized linear model (GLM) analysis was conducted on the BOLD signal obtained during the period of time (4 s) when subjects received monetary feedback; either 'reward' or 'punishment'. The clusters of voxels that showed a greater response to 'reward' compared to 'punishment' at group-level were reported. The analyses were thresholded at $p < .001$ (uncorrected) with cluster size above 40 voxels.
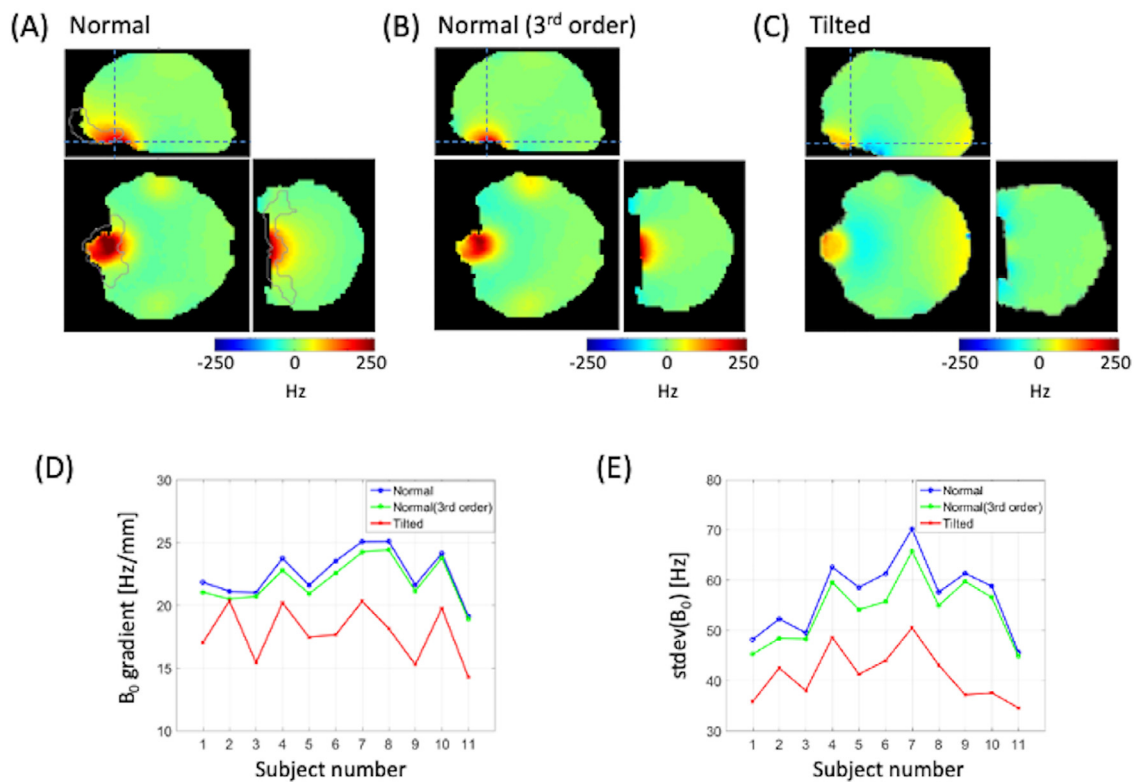
4. Results

4.1. Simulation

Fig. 1B shows the simulated susceptibility-induced B_0 distribution in the head at different applied field directions. As reported previously (Heberlein and Hu, 2001; Tyszka and Mamelak, 2002), the region of strong positive B_0 in the prefrontal region is pushed anteriorly as θ increases. This is accompanied by the appearance of weaker, negative B_0 near the midbrain. Quantitatively, Fig. 1C (blue trace) shows the maximum B_0 gradient in the elliptical ROI drawn in Fig. 1B, indicating about 30% reduction from $\theta = 0°$ to 50°. The standard deviation of B_0 in the same ROI is more than halved at $\theta = 50°$ (Fig 1D, blue trace) before eventually turning upward as the negative B_0 enters the ROI.

4.2. B_0 map

For all eleven subjects tested, B_0 homogeneity was clearly improved in the PFC region. As an example, Fig. 3A–C compares the 3-plane B_0 maps at the two head orientations and the normal-orientation 3rd order shim simulation result for a representative subject. B_0 spatial variation in the PFC in the tilted condition was greatly reduced compared to the normal condition. The head-tilted B_0 map exhibited slight degradation of homogeneity in the occipital bone area, which is in agreement with numerical simulation (Fig. 1B). Fig. 3D shows the peak B_0 gradient values in the orbital gyrus ROI at the two head orientations for all subjects. On average, the peak B_0 gradient was reduced only by 2.7% in the 3rd order shim simulation, while it was reduced by 21% by head tilting.

Fig. 3. (A–C). Measured B_0 maps at normal (A) and tilted (C) head orientations for subject 9 (tilt angle = 53°). The result of the 3rd order shim simulation is shown in (B). The solid gray lines in (A) indicate the orbital gyrus ROI boundary. The dashed crossing lines indicate the locations of the axial and coronal slices. (D-E). Plots of the peak B_0 gradient (D) and B_0 standard deviation (E) in the orbital gyrus at two head orientations for all subjects in Experiment 1.

Tilted-head scan also resulted in substantial decrease (mean 27%) in B_0 standard deviation for all subjects (Fig. 3E), superior to the reduction achieved by the 3rd order shimming (5.1%).

4.3. Multi-echo gradient echo scans

Fig. 4A–B compares the multi-echo gradient echo magnitude images from a representative subject. Even at the high-resolution of $0.53 \times 0.53 \times 0.8$ mm³, the susceptibility-induced signal dropout and image quality degradation in the PFC region are clear for the normal orientation scan at TE = 32 and 42 ms. The artifacts are largely removed in the head-tilted scan (Fig 4B), where images at different TEs exhibit more consistent image qualities compared to the normal orientation scan. The R_2^* maps reconstructed from the magnitude images in each orientation are shown in Fig. 4C and D. As expected, strongly inflated R_2^* values are apparent in the signal drop-out region (red line in Fig. 4C). Fig. 4E presents the TE-dependent signal decay in the corresponding regions in both orientations for all subjects in Experiment 2. It is apparent that head tilting successfully suppressed abrupt signal drop-outs in later echoes, enabling more reliable R_2^* measurements. The mean ± standard deviation (across the subjects) of R_2^* in the signal drop-out region was 51.7 ± 6.4 (normal) and 17.3 ± 1.9 (tilted). A significant difference between the orientations was observed in a paired t-test. ($p = 0.00015$)

4.4. Functional MRI

#### 4.4.1. Comfort survey, head motion, and behavioral task performance

All subjects reported that normally positioned scans were more comfortable than head-tilted scans for both Experiment 1 (scores for normal: 4.58 ± 0.51, tilted: 2.75 ± 0.62) and Experiment 2 (normal: 4.67 ± 0.52, tilted: 3.50 ± 0.84, reported on a scale of 1 to 5) (see Supplementary Table S1 for details). In addition to the possible neck strain, additional

restraining pads under the neck and above the head, possible contact between the chin and the coil housing, and reduced room for hand and arm movement due to the elevated torso may have contributed to the discomfort in the head-tilted scan. None of the subjects, however, reported severe discomfort (scale 1, 'very uncomfortable'), nor stopped the scan during the head-tilted scan. The amount of subjects' head motion was compared between the two orientations. For all 6 motion parameters, less head motion was observed during the head-tilted scan compared to the normal orientation scan in task-based fMRI (all FDR-ps < .0001; Supplementary Table S2). A similar decrease in motion for the head-tilted scan was also observed in rest fMRI, though it did not survive multiple comparisons correction (all FDR-ps < .31). Such a decrease is presumably due to added padding around the head during the head-tilted scan.

We have also examined whether the behavioral task performance in the tilted orientation scan was comparable to the normally positioned scan. Interestingly, we observed an increase in subjects' task performance during the tilted scans. The percentage of receiving reward increased from 49.8% in the normal orientation scan to 55.7% in the tilted scan ($t(10) = 4.81, p < .001$). The average reaction time (RT) for the trial-by-trial binary choice of the stimulus was faster in the tilted, compared to the normal orientation scan ($t(10) = 4.70, p < .0001$). The results suggest a possibility that the subjects remained more alert to the task during the head-tilted scan compared to the normal scan. These observations are compatible with our hypothesis that the head-tilted posture was not overly distracting nor stressful to the subjects when performing cognitive tasks.

4.4.2. EPI tSNR improvement in the PFC region

Fig. 5 shows the axial and sagittal views of a single subject's EPI. The benefit of the head-tilted scan (Fig. 5B) is clearly appreciable from the disappearance of a characteristic 'V-shaped' signal loss in the inferior part of the prefrontal region in normal orientation EPI (Fig. 5A). Using a mask manually drawn on each subject similar to the one shown
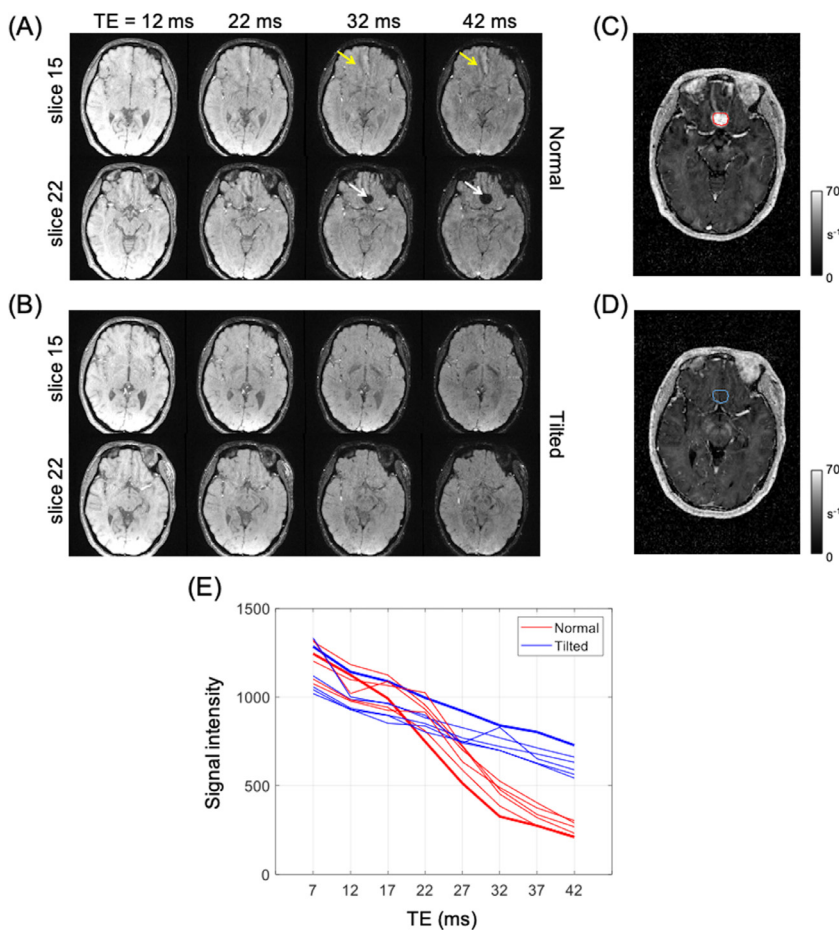
Fig. 4. Comparison of multi-echo gradient echo magnitude images on an exemplar subject of Experiment 2 (tilt angle = 44°). Two axial slices (slice 15 and 22), 7 mm apart, are shown at TE = 12, 22, 32, and 42 ms for normal (A) and tilted (B) orientation scans. Signal loss (white arrows) and image quality degradation (yellow arrows) are clear for TE = 32 ms and 42 ms in (A). (C) and (D) show the normal and tilted orientation R_2^* maps on slice 22. The decay of the mean signal intensity in the regions marked by the red (C) and blue (D) lines for both orientations is shown in (E) with thick red and blue lines, respectively. The corresponding decay curves for all other (five) subjects are indicated in thin lines.
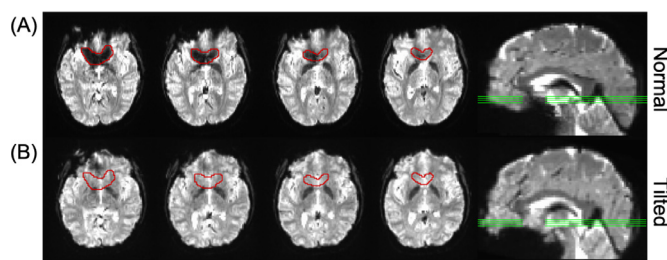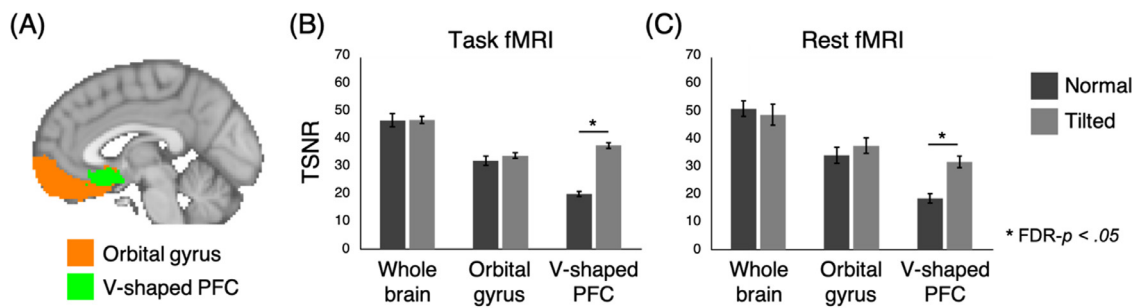

Fig. 5. The EPI intensities of an exemplar subject in normal (A) and tilted (B) orientations displayed on the same grey scale (tilt angle = 52°). The locations of the 4 axial slices are indicated in green lines on the sagittal images on the right. The 'V-shaped' regional mask was drawn manually to indicate an area that shows signal loss in the prefrontal cortex (red contour). The characteristic 'V-shaped' region of signal loss in the normal orientation scan is not seen in the head-tilted scan.

ference in tSNR across the whole brain mask (task fMRI: $t(10) = 0.05$, FDR-$p = .964$; rest fMRI: $t(5) = 0.86$, FDR-$p = .429$). In the orbital gyrus, the tSNR showed a trend of increase in the tilted compared to the normal orientation scans for both task fMRI ($t(10) = 1.25$, FDR-$p = .361$) and rest fMRI ($t(5) = 1.34$, FDR-$p = .357$), though not to a significant degree. Our observation indicates that the improved B_0 homogeneity in the orbitofrontal region by head tilting translates to significant local enhancement of tSNR of EPI in the PFC region.

4.4.3. fMRI activation

We examined whether we could observe comparable modulation of BOLD responses across different head orientations while a cognitive task is performed. Using GLM, we identified regions that were significantly activated by rewards compared to punishments as subjects participated in the probabilistic reversal learning task. For the head-tilted scan, clusters of voxels within the left posterior cingulate cortex (PCC) [+4.9 +43.8 +40.6], bilateral precuneus (PreCu) [+0.5 +66.8 +27.6], bilateral medial frontal gyrus (mFG) [-2.4 -55.3 -8.4], and bilateral anterior cingulate cortex (ACC) [+0.4 -41.7 -6.2] were significantly more activated when receiving rewards compared to receiving punishments (uncorrected $p < .001$, cluster size > 40; Fig. 7C). The previous findings that used the same experimental paradigm and analyses were replicated in the head-tilted fMRI (Fig. 7A; Bray et al., 2010; O'Doherty et al., 2001). Activation in the frontal region was also replicated in normal orientation fMRI. Our finding suggests that the head-tilted scan is not only implementable during task fMRI but also capable of producing reliable experimental results.

in Fig. 5B, we found that the mean signal (averaged over the subjects) significantly increased in the tilted orientation compared to the normal orientation in both task fMRI ($t(10) = 8.01$, FDR-$p < .0001$; Supplementary Fig. 1A) and rest fMRI ($t(5) = 14.86$, FDR-$p < .001$; Supplementary Fig 1B). Furthermore, the temporal SD decreased in the tilted orientation compared to the normal orientation, in task fMRI ($t(10) = 5.78$, FDR-$p < .001$; Supplementary Fig. 1C). The decrease was also observed, albeit to a lesser degree, in rest fMRI ($t(5) = 1.73$, FDR-$p = .354$; Supplementary Fig. 1D). Consequently, the tSNR in the masked PFC region showed strong improvement in the head-tilted compared to the normal condition for both task fMRI ($t(10) = 14.42$, FDR-$p < .0001$; Fig. 6B) and rest fMRI ($t(5) = 7.92$, FDR-$p < .01$; Fig. 6C). We observed no dif-

Fig. 6. Temporal signal-to-noise ratio (tSNR, averaged across the subjects) of the EPI images. (A) Regional masks used to calculate tSNR. The 'V-shaped PFC' mask shows the voxels that were manually selected in more than half of the subjects in Experiment 1. (B,C) The tSNR of the 'V-shaped PFC' region was higher in the head-tilted compared to the normally oriented condition in both task (B) and rest (C) fMRI ($p < .05$, corrected for multiple comparisons using false discovery rate (FDR)).
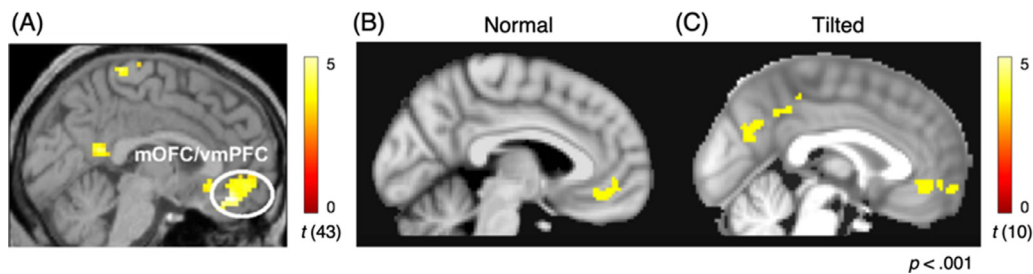
Fig. 7. Task-based functional MRI results. (A) Reward vs. punishment contrast reported in a previous study that used a probabilistic reversal learning task ($p < .001$). Adapted from Bray et al. (2010) with permission. mOFC, medial orbitofrontal cortex; vmPFC, ventromedial prefrontal cortex. Reward vs. punishment contrast in the normal (B) and tilted (C) orientation scans of the current study where the same probabilistic reversal learning task was used ($p < .001$, cluster size > 40 voxels, $N = 11$).

5. Discussion

We have tested the feasibility of head-tilted brain imaging as a means to reduce the susceptibility-induced B_0 gradient and gradient-echo signal loss in the PFC. We have confirmed earlier reports (Heberlein and Hu, 2001; Tyszka and Mamelak, 2002) that increasing the head pitch angle improves B_0 shimming in the PFC and demonstrated that this translates into higher image quality in multi-echo gradient echo imaging and EPI without any modifications to the hardware, sequence, and post-processing. We found that raising the subjects' back by 10 cm or more greatly facilitates implementation of large-angle head tilting, resulting in all seventeen subjects recruited reporting acceptable scan experience during >20 min head-tilted scan sessions, some including a cognitive task-driven fMRI scan. This leads us to believe that the proposed chin-up head position was not overly distracting, and is probably usable in other functional and anatomical neuroimaging studies involving the orbitofrontal region.

Many authors have proposed methods to address the EPI signal dropout in the orbitofrontal cortex through improved shimming. Compared to other shimming methods targeting sinus/nasal cavity-induced fields (Cusack et al., 2005; Hsu and Glover, 2005; Juchem et al., 2010; Yang et al., 2011), the head-tilting method is unique in that it uses the shape of the cavity-induced field itself to improve shimming. Such approach can potentially do a better job in compensating subject-specific high-order B_0 variations than shim coil-based approaches. We found that chin-up head tilting did not severely degrade shimming in other regions of the brain.

Our 20-channel head-and-neck coil provided acceptable signal-to-noise ratio while accommodating relatively large head-tilt angles for the subjects scanned. While the design and tuning of the coil elements were most likely optimized for the best SNR in normal orientation scans, we found that the whole-head EPI tSNR did not differ significantly between the tilted and normal conditions. On the contrary, the signal intensity and tSNR in the small orbitofrontal region vulnerable to signal loss in conventional EPI were clearly enhanced when the head was tilted, an effect dominated by improved B_0 shimming and recovery of the signal near the nasal cavity in the head-tilted scans. This suggests that in the future, a custom-designed brain coil with flexible table mount could potentially enable head-tilted imaging with better tSNR while increasing the subject's comfort, to benefit e.g., task-based fMRI focused on the orbitofrontal region.

Improved image quality for multi-echo gradient echo imaging and EPI in the orbitofrontal region should enable more accurate measurements of R_2^* and functional activation, respectively. It should be noted, however, that both R_2^* and BOLD fMRI contrast in the brain are known to depend on the orientation of the tissue and the blood vessels with respect to the main magnetic field (Kim and Ogawa, 2012). This means that the "true" R_2^* and BOLD contrast may differ between normal and head-tilted scans, making direct comparison of their measurements difficult to interpret. Likewise, such orientation dependence makes it difficult to compare the parameters among different subjects if they are obtained with different head tilt angles. For comparative studies, therefore, it is recommended that the tilt angle be controlled across the subjects as much as practical. On the other hand, head-tilted imaging on a given subject at multiple angles could be used to study MR contrast anisotropy, which can provide insight into the tissue microstructure (Aggarwal et al., 2016).

Our task-based fMRI results showed that all participants were able to complete cognitive tasks without reporting severe discomfort with head tilting. Additionally, head-tilted scan resulted in significantly decreased head motion as well as improved cognitive task performance, presumably due to an increased attentional focus as the participants were positioned in an unusual posture during the scan. Further, the observed BOLD activation pattern was comparable to the previous reports (Bray et al., 2010). Overall, we found that the head-tilted brain scan can be made compatible with standard behavioral and neuroimaging

studies, producing robust functional signals with benefits in PFC signal recovery.

Our study had several limitations. First, the tilt angles were not precisely controlled, and the angle dependence of the image quality was not systematically investigated. Instead, we focused on probing the salient difference between normal and head-tilted scans and investigated the practicality of the latter. As a natural extension of the present study, it is worthwhile to examine the shim and the tSNR improvement as a function of the tilt angle for individual subjects. Such study will be useful to determine the best trade-off between improved shimming and subject comfort. Second, we have tested the head-tilted scan only with the basic multi-echo gradient echo and EPI sequences. While these sequences were chosen because of their widespread use in neuroimaging and in our institute, we believe that the improved B_0 homogeneity achieved by head-tilting will benefit other B_0-sensitive sequences as well, such as those for the balanced steady-state free precession and spectroscopy. In addition, phase-based quantitative imaging such as QSM (Liu et al., 2009; Wang and Liu, 2015) is expected to benefit from reduced phase wraps in the PFC region in head-tilted scans. Finally, we have collected data from a relatively small number of volunteers who were young, healthy, and cooperating. Raising the torso and tilting back the head may not be compatible with scans on obese subjects or patients with muscle stiffness. We do not envision that the proposed method could be easily translated to the clinic; rather, we propose that the improved shimming by head tilting could help enhance certain normal-subject neuroimaging studies on a subset of the population.

In conclusion, we have demonstrated that for the healthy volunteers tested, back-raised and chin-up head-tilted brain imaging can provide substantial benefits in B_0 shimming and gradient-echo signal recovery in the PFC. Maintaining a tilt angle approaching the magic angle was feasible for at least 20 min with modest change in subject handling logistics using a clinical head-neck array coil. The method can be used synergistically with conventional shim strategies, as well as sequence-based signal recovery techniques in gradient echo-based neuroimaging scans.

Declaration of Competing Interest

The authors have no relevant conflicts of interest to disclose.

Funding

Supplementary materials

Supplementary material associated with this article can be found, in the online version, at doi:10.1016/j.neuroimage.2020.117265.

References

Aggarwal, M., Kageyama, Y., Li, X., Van Zijl, P.C., 2016. B0-orientation dependent magnetic susceptibility-induced white matter contrast in the human brainstem at 11.7 T. Magn. Reson. Med. 75, 2455–2463.
Brainard, D.H., 1997. The psychophysics toolbox. Spat. Vis. 10, 433–436.
Bray, S., Shimojo, S., O'Doherty, J.P., 2010. Human medial orbitofrontal cortex is recruited during experience of imagined and real rewards. J. Neurophysiol. 103, 2506–2512.
Cheng, Y.-C.N., Neelavalli, J., Haacke, E.M., 2009. Limitations of calculating field distributions and magnetic susceptibilities in MRI using a Fourier based method. Phys. Med. Biol. 54, 1169.
Clare, S., Evans, J., Jezzard, P., 2006. Requirements for room temperature shimming of the human brain. Magn. Reson. Med. 55, 210–214.
Constable, R.T., 1995. Functional MR imaging using gradient-echo echo-planar imaging in the presence of large static field inhomogeneities. J. Magn. Reson. Imaging 5, 746–752.
Constable, R.T., Spencer, D.D., 1999. Composite image formation in z-shimmed functional MR imaging. Magn. Reson. Med. 42, 110–117.
Cox, R.W., 1996. AFNI: software for analysis and visualization of functional magnetic resonance neuroimages. Comput. Biomed. Res. 29, 162–173.
Cusack, R., Russell, B., Cox, S.M., De Panfilis, C., Schwarzbauer, C., Ansorge, R., 2005. An evaluation of the use of passive shimming to improve frontal sensitivity in fMRI. Neuroimage 24, 82–91.
Deichmann, R., Gottfried, J.A., Hutton, C., Turner, R., 2003. Optimized EPI for fMRI studies of the orbitofrontal cortex. Neuroimage 19, 430–441.
Du, Y.P., Dalwani, M., Wylie, K., Claus, E., Tregellas, J.R., 2007. Reducing susceptibility artifacts in fMRI using volume-selective z-shim compensation. Magn. Reson. Med. 57, 396–404.
Fan, L., Li, H., Zhuo, J., Zhang, Y., Wang, J., Chen, L., Yang, Z., Chu, C., Xie, S., Laird, A.R., 2016. The human brainnetome atlas: a new brain atlas based on connectional architecture. Cereb. Cortex 26, 3508–3526.
Glover, G.H., 1999. 3D z-shim method for reduction of susceptibility effects in BOLD fMRI. Magn. Reson. Med. 42, 290–299.
Heberlein, K., Hu, X., 2001. Improved shim by subject head positioning. In: Proceedings of the 9th Annual Meeting of ISMRM. Glasgow, Scotland.
Hsu, J.J., Glover, G.H., 2005. Mitigation of susceptibility-induced signal loss in neuroimaging using localized shim coils. Magn. Reson. Med. 53, 243–248.
Jenkinson, M, Beckmann, CF, Behrens, TE, Woolrich, MW, Smith, SM, 2012. FSL. Neuroimage 62 (2), 782–790. doi:10.1016/j.neuroimage.2011.09.015.
Jenkinson, M., Wilson, J.L., Jezzard, P., 2004. Perturbation method for magnetic field calculations of nonconductive objects. Magn. Reson. Med. 52, 471–477.
Juchem, C., Nixon, T.W., McIntyre, S., Rothman, D.L., de Graaf, R.A., 2010. Magnetic field homogenization of the human prefrontal cortex with a set of localized electrical coils. Magn. Reson. Med. 63, 171–180.
Kim, P., Lim, J., Ahn, C., 2007. Higher order shimming for ultra-fast spiral-scan imaging at 3 tesla MRI system. J. Korean Soc. Magn. Reson. Med. 11, 95.
Kim, S.-G., Ogawa, S., 2012. Biophysical and physiological origins of blood oxygenation level-dependent fMRI signals. J. Cereb. Blood Flow Metab. 32, 1188–1206.
Lee, S.K., Hwang, S.H., Barg, J.S., Yeo, S.J., 2018. Rapid, theoretically artifact-free calculation of static magnetic field induced by voxelated susceptibility distribution in an arbitrary volume of interest. Magn. Reson. Med. 80, 2109–2121.
Liu, T., Spincemaille, P., De Rochefort, L., Kressler, B., Wang, Y., 2009. Calculation of susceptibility through multiple orientation sampling (COSMOS): a method for conditioning the inverse problem from measured magnetic field map to susceptibility source image in MRI. Magn. Reson. Med. 61, 196–204.
O'Doherty, J., Kringelbach, M.L., Rolls, E.T., Hornak, J., Andrews, C., 2001. Abstract reward and punishment representations in the human orbitofrontal cortex. Nat. Neurosci. 4, 95–102.
Pelli, D.G., 1997. The VideoToolbox software for visual psychophysics: Transforming numbers into movies. Spat. Vis. 10, 437–442.
Power, J.D., Barnes, K.A., Snyder, A.Z., Schlaggar, B.L., Petersen, S.E., 2012. Spurious but systematic correlations in functional connectivity MRI networks arise from subject motion. Neuroimage 59, 2142–2154.
Power, J.D., Mitra, A., Laumann, T.O., Snyder, A.Z., Schlaggar, B.L., Petersen, S.E., 2014. Methods to detect, characterize, and remove motion artifact in resting state fMRI. Neuroimage 84, 320–341.
Schweser, F., Deistung, A., Lehr, B.W., Reichenbach, J.R., 2011. Quantitative imaging of intrinsic magnetic tissue properties using MRI signal phase: an approach to in vivo brain iron metabolism? Neuroimage 54, 2789–2807.
Segars, W.P., Sturgeon, G., Mendonca, S., Grimes, J., Tsui, B.M., 2010. 4D XCAT phantom for multimodality imaging research. Med. Phys. 37, 4902–4915.
Sengupta, S., Welch, E.B., Zhao, Y., Foxall, D., Starewicz, P., Anderson, A.W., Gore, J.C., Avison, M.J., 2011. Dynamic B0 shimming at 7 T. Magn. Reson. Imaging 29, 483–496.
Tyszka, J.M., Mamelak, A.N., 2002. Quantification of B0 homogeneity variation with head pitch by registered three-dimensional field mapping. J. Magn. Reson. 159, 213–218.
Valette, J., Guillermier, M., Besret, L., Boumezbeur, F., Poupon, C., Amadon, A., Hantraye, P., Lebon, V., 2006. B0 homogeneity throughout the monkey brain is strongly improved in the sphinx position as compared to the supine position. Magn. Reson. Med. 23, 408–412.
Wang, Y., Liu, T., 2015. Quantitative susceptibility mapping (QSM): decoding MRI data for a tissue magnetic biomarker. Magn. Reson. Med. 73, 82–101.
Yang, S., Kim, H., Ghim, M.-O., Lee, B.-U., Kim, D.-H., 2011. Local in vivo shimming using adaptive passive shim positioning. Magn. Reson. Imaging 29, 401–407.
Yang, Y.-J., Yoon, J.-H., Baek, H.-M., Ahn, C.-B., 2018. Simultaneous unwrapping phase and error recovery from inhomogeneity (super) for quantitative susceptibility mapping of the human brain. Investig. Magn. Reson. Imaging 22, 37–49.
Yoder, D.A., Zhao, Y., Paschal, C.B., Fitzpatrick, J.M., 2004. MRI simulator with object-specific field map calculations. Magn. Reson. Imaging 22, 315–328.